






# Water UV-shielding in the Terrestrial Planet-forming Zone: Implications for Oxygen-18 Isotope Anomalies in H<sub>2</sub><sup>18</sup>O Infrared Emission and Meteorites

Jenny K. Calahan , Edwin A. Bergin , and Arthur D. Bosman   
University of Michigan, 323 West Hall, 1085 South University Avenue, Ann Arbor, MI 48109, USA  
Received 2022 April 1; revised 2022 June 15; accepted 2022 July 3; published 2022 July 25

## Abstract

An understanding of abundance and distribution of water vapor in the innermost region of protoplanetary disks is key to understanding the origin of habitable worlds and planetary systems. Past observations have shown H<sub>2</sub>O to be abundant and a major carrier of elemental oxygen in disk surface layers that lie within the inner few astronomical units of the disk. The combination of high abundance and strong radiative transitions leads to emission lines that are optically thick across the infrared spectral range. Its rarer isotopologue H<sub>2</sub><sup>18</sup>O traces deeper into this layer and will trace the full content of the planet-forming zone. In this work, we explore the relative distribution of H<sub>2</sub><sup>16</sup>O and H<sub>2</sub><sup>18</sup>O within a model that includes water self-shielding from the destructive effects of ultraviolet radiation. In this Letter we show that there is an enhancement in the relative H<sub>2</sub><sup>18</sup>O abundance high up in the warm molecular layer within 0.1–10 au due to self-shielding of CO, C<sup>18</sup>O, and H<sub>2</sub>O. Most transitions of H<sub>2</sub><sup>18</sup>O that can be observed with JWST will partially emit from this layer, making it essential to take into account how H<sub>2</sub>O self-shielding may effect the H<sub>2</sub>O to H<sub>2</sub><sup>18</sup>O ratio. Additionally, this reservoir of H<sub>2</sub><sup>18</sup>O-enriched gas in combination with the vertical “cold finger” effect might provide a natural mechanism to account for oxygen isotopic anomalies found in meteoritic material in the solar system.

*Unified Astronomy Thesaurus concepts:* [Protoplanetary disks \(1300\)](#); [Astrochemistry \(75\)](#)

## 1. Introduction

It is expected that the vast majority of solar-type stars host an exoplanet within 1 au (Johnson et al. 2010; Mulders et al. 2018). As a result, it can be assumed that the inner gaseous region of protoplanetary disks must be a hospitable environment for active planet formation. Typical temperatures place nearly all primary volatile carriers of carbon, nitrogen, and oxygen into the gas within surface layers providing a rich environment for astronomical observations and constraint (Pontoppidan et al. 2014). Volatiles (i.e., CO, H<sub>2</sub>O, CO<sub>2</sub>) are potential starting points for the creation of complex molecules and the ice coatings of preplanetary pebbles (Wang et al. 2005; Gundlach & Blum 2015). These simple precursors have been widely observed toward gas-rich disks within the 0.1–10 au region around young stars using the Spitzer space telescope (i.e., Carr & Najita 2008; Pontoppidan et al. 2010; Salyk et al. 2011). Mapping the spatial extent and abundance of volatile molecules within the inner disk is essential knowledge used to piece together the connection between the chemical reservoir of a gas-rich disk and the resulting planets.

The JWST mission will provide improved spectral resolution access to the inner disk region (JWST–MIRI:  $\lambda/\Delta\lambda = 2000\text{--}3000$ ; Rieke et al. 2015), as compared to Spitzer’s InfraRed Spectrograph ( $\lambda/\Delta\lambda = 600$ ; Houck et al. 2004). Nearly 50 disks will be targeted in the first set of JWST observations and will be used to enhance the study of emissions from volatiles in the terrestrial planet-forming zone. One molecule of high scientific impact is H<sub>2</sub>O. Based on previous observations and theoretical work, it is expected that H<sub>2</sub>O will be in high enough abundance such that its emission is optically thick (Carr &

Najita 2008). The lesser abundant isotopologue H<sub>2</sub><sup>18</sup>O is also observable with JWST instruments and, with reduced optical depth for its emission lines, will be used to infer the abundance and distribution of H<sub>2</sub>O using the ratio between <sup>16</sup>O and <sup>18</sup>O.

The most frequently used value for <sup>16</sup>O/<sup>18</sup>O is 550. This value comes from Wilson (1999), and is the average observed ratio for five local interstellar medium (ISM) sources. This ratio has been seen to vary across the Galaxy following

$$(^{16}\text{O}/^{18}\text{O}) = (58.8 \pm 11.8)D_{\text{GC}} + (37.1 \pm 82.6), \quad (1)$$

where  $D_{\text{GC}}$  is the distance of a source from the Galactic center (Wilson & Rood 1994). Within the environment of a protoplanetary disk, however, there are chemical processes that can alter this ratio.

One such process is molecular self-shielding. Self-shielding is a process via which molecules, such as CO, N<sub>2</sub>, and H<sub>2</sub>, can protect themselves further from the source of radiation from the destructive effects of photodissociation from ultraviolet photons (van Dishoeck & Black 1988). These molecules are dissociated via a line process, as opposed to molecules with photodissociation cross sections that are continuous at UV wavelengths (Heays et al. 2017). Thus, molecules closer to the radiation source can absorb UV photons allowing for the lines to become optically thick and, hence, self-shield molecules downstream from the source of UV photons. CO self-shielding can occur in gas-rich disks leading to a relative overabundance of <sup>12</sup>C<sup>16</sup>O compared to <sup>12</sup>C<sup>18</sup>O and <sup>12</sup>C<sup>17</sup>O in the warm disk region (Miotello et al. 2014) because the absorbing lines of the lesser abundant isotopologues have reduced opacity. This process can help explain relatively high C<sup>16</sup>O/C<sup>18</sup>O ratios that have been observed in a handful of protoplanetary disks (i.e., Brittain et al. 2005; Smith et al. 2009) and potentially might contribute to isotopic anomalies detected in asteroids and comets as compared to our Sun (Lyons & Young 2005; Nittler & Gaidos 2012; Altwegg et al. 2020).

Bethell & Bergin (2009) demonstrated that, because of fast formation rates in hot ( $>400$  K) gas, water can also self-shield. Further, this shielding is unique in that it not only shields itself, but shields over a wide range of wavelength space, similar to ozone in the Earth’s atmosphere. Thus, water might also operate as a shield for other molecules, a process we call water UV-shielding. The combination of CO self-shielding and H<sub>2</sub>O UV-shielding could produce an environment where the H<sub>2</sub>O, H<sub>2</sub><sup>18</sup>O, and CO are protected while C<sup>18</sup>O continues to photodissociate. In this <sup>18</sup>O-rich environment, H<sub>2</sub><sup>18</sup>O will form and continue to be protected, raising the relative abundance of H<sub>2</sub><sup>18</sup>O with respect to H<sub>2</sub>O in specific surface layers. This could have a strong impact on both the CO/C<sup>18</sup>O and H<sub>2</sub>O/H<sub>2</sub><sup>18</sup>O values, altering them drastically from what is expected within the average ISM. These ratios will be commonly used in future JWST observations due to the expected high optical depth of CO and H<sub>2</sub>O within the inner disk. Additionally, the spatial extent of any <sup>18</sup>O-rich environment relative to where observed H<sub>2</sub><sup>18</sup>O and H<sub>2</sub>O lines emit from will have a strong effect on the determination of H<sub>2</sub>O abundance within protoplanetary disks. Having accurate isotopic conversation factors could be critical as it is possible that the inner disk could betray evidence of volatile enhancements due to pebble drift (Ciesla & Cuzzi 2006; Banzatti et al. 2020).

One final consideration to the chemical make-up of the inner disk is Ly $\alpha$  radiation. The Ly $\alpha$  transition often contains the vast majority of the energy within the far-UV (FUV) range if present in a stellar spectrum of T Tauri stars (Herczeg et al. 2002; Schindhelm et al. 2012). It is readily observed toward young stars that are actively accreting and possess a gas-rich disk. The Ly $\alpha$  transition occurs at 1216 Å and can photodissociate water (van Dishoeck et al. 2006). Ly $\alpha$  is not often taken into account in radiation transfer codes, due to its added complexity of not only scattering off of dust but also atomic hydrogen, causing the Ly $\alpha$  photons to scatter isotropically below the hot atomic layer of the disk (Bethell & Bergin 2011). To explore the strength that both water and CO self-shielding will have on the oxygen isotopic ratio, Ly $\alpha$  needs to be accounted for.

This Letter is a companion to Bosman et al. (2022) and S. Duval et al. (2022, in preparation). Bosman et al. (2022) set up protoplanetary disk models focused on the innermost region that take into account water UV-shielding and efficient chemical heating processes. These two processes are required in order for a thermochemical calculation to reproduce water line emission and observed excitation temperatures from Spitzer. Using the same modeling setup, Bosman et al. (2022) show that CO<sub>2</sub>-to-H<sub>2</sub>O ratios can also be achieved, strengthened by additional depletion of excess oxygen beyond the water snowline. S. Duval et al. (2022, in preparation) will focus on the impact of water UV-shielding on the chemical composition of the terrestrial planet-forming region.

In this Letter we will explore the abundances of both H<sub>2</sub>O and H<sub>2</sub><sup>18</sup>O in the innermost few astronomical units of protoplanetary disks where the excitation conditions are favorable for detection of rotational and vibrational emissions at mid-infrared wavelengths. This exploration will use the Spitzer observational legacy as a constraint (Pontoppidan et al. 2010; Salyk et al. 2011), but look forward to JWST observations that will be observing systems where both Ly $\alpha$  radiation and water UV-shielding will be present.

## 2. Methods

### 2.1. Thermochemical Modeling: DALI

Dust And Lines (DALI) is a physical–chemical code that accounts for radiation transfer and thermal and chemical calculations throughout a disk (Bruderer et al. 2012; Bruderer 2013). It contains an isotope chemical network (Miotello et al. 2014) and accounts for molecular self-shielding. For this project, H<sub>2</sub>O UV-shielding has been additionally accounted for; see Bosman et al. (2022) for details. We utilize a model derived from the AS 209 and corresponding stellar spectrum from Zhang et al. (2021), and explore the effect of H<sub>2</sub>O UV-shielding and Ly $\alpha$  radiation in a flat versus thick model and two levels of dust settling. We include the <sup>18</sup>O isotopologue of every oxygen-carrying species in our chemical network.

After an initial radiative transfer calculation, thermal balance, and chemical abundance distribution determination, we account for Ly $\alpha$  radiation using another code, detailed in the following section. The results from the separate Ly $\alpha$  radiative transfer calculation are combined with the initial disk radiation field as calculated by DALI. We then calculate a new thermal balance and chemical environment, containing the final distribution of H<sub>2</sub>O and H<sub>2</sub><sup>18</sup>O.

Excitation data for both ortho- and para-H<sub>2</sub><sup>18</sup>O were compiled into a file identical to the format from the Leiden LAMDA database (Schöier et al. 2005).<sup>1</sup> Line excitation data were obtained via the HITRAN database (Gordon et al. 2022)<sup>2</sup> and collisional data from the H<sub>2</sub><sup>16</sup>O LAMDA file (Faure & Josselin 2008). This was used for ray-tracing calculations with DALI to determine which lines may be observable and from where in the disk they emit.

### 2.2. Inclusion of Ly $\alpha$

The inclusion of the Ly $\alpha$  is derived from a radiation transfer code described by Bethell & Bergin (2011). Briefly, this code calculates the transport of both FUV-continuum and Ly $\alpha$  photons. FUV photons are solely affected by the dust distribution, while Ly $\alpha$  is additionally affected by resonance line scattering. An initial distribution of H and H<sub>2</sub> is derived using the thermochemical calculation from DALI, and Ly $\alpha$  propagates throughout the distribution of gas and dust, scattered by atomic H in the H-rich layer, and eventually scattered and absorbed by dust.

After this calculation, the Ly $\alpha$ -affected radiation field is combined with the DALI radiation field. The effects of a separate stellar input spectrum are normalized out of the Ly $\alpha$  radiative transfer results, and a depletion or enhancement factor across wavelengths covered by the Ly $\alpha$  line and its line wings is calculated. The original DALI radiation field contains Ly $\alpha$  emission as it would exist if Ly $\alpha$  photons scattered normally off of small dust grains only, identically to continuum-UV photons.

## 3. Results

### 3.1. H<sub>2</sub><sup>18</sup>O-enhanced Region

We find an H<sub>2</sub><sup>18</sup>O-rich environment high up in the molecular region of the disk. Enhanced H<sub>2</sub><sup>18</sup>O exists in models that range

<sup>1</sup> <https://home.strw.leidenuniv.nl/~moldata/>

<sup>2</sup> <https://hitran.org/>

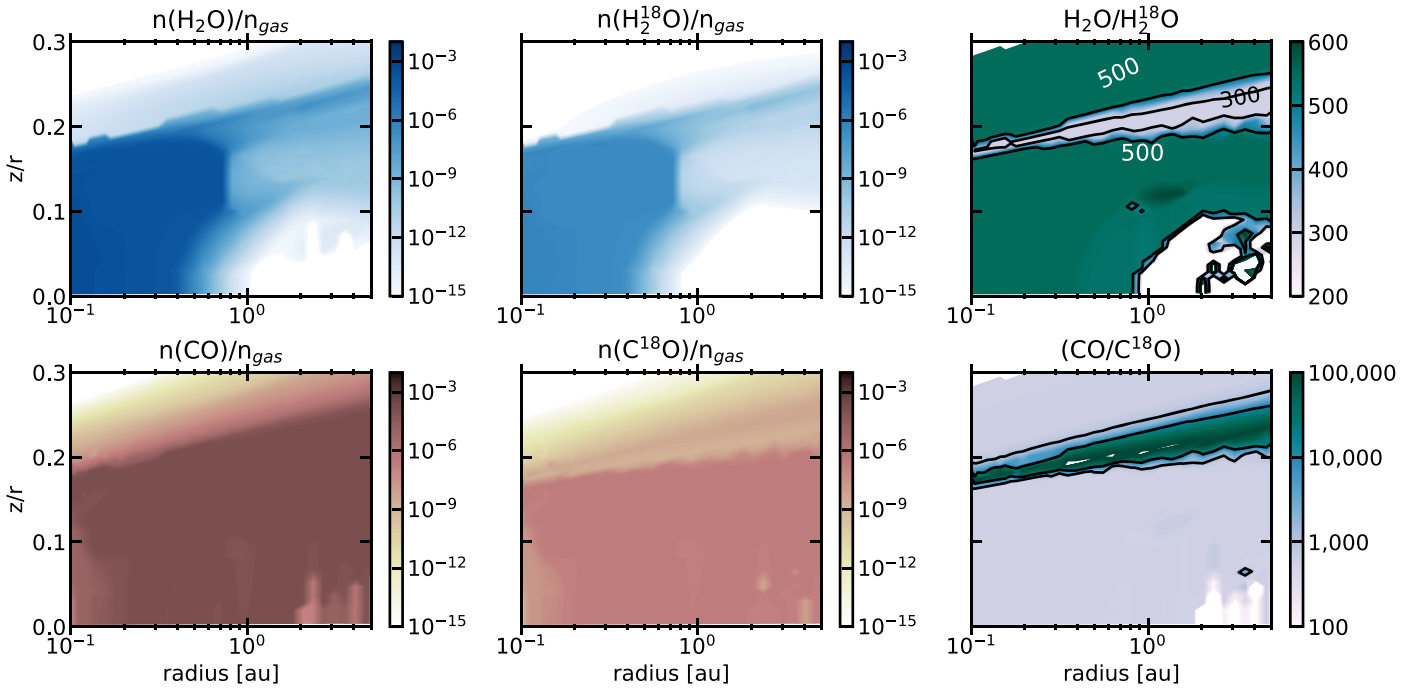


**Figure 1.** The  $\text{H}_2\text{O}$ ,  $\text{H}_2^{18}\text{O}$ ,  $\text{CO}$ , and  $\text{C}^{18}\text{O}$  abundance in units of  $(\text{mol}/\text{cm}^{-3})/n_{\text{gas}}$  throughout the inner disk (left and center plots), and the ratio between  $\text{H}_2\text{O}$  and  $\text{H}_2^{18}\text{O}$  (top right) and  $\text{CO}$  and  $\text{C}^{18}\text{O}$  (bottom right). At  $z/r \approx 0.2$  a unique region exists where  $\text{H}_2^{18}\text{O}$  is enhanced and  $\text{C}^{18}\text{O}$  is greatly depleted.

in flaring angle and dust settling parameters. Four models were explored with two different values for scale height and dust settling, and these individual models are detailed in the Appendix of Bosman et al. (2022). The following figures and discussion are based on the flattest and most highly settled model, which reproduce  $\text{H}_2\text{O}$  and  $\text{CO}_2$  spectra simultaneously (see Bosman et al. 2022). In this model, a region where  $\text{H}_2\text{O}/\text{H}_2^{18}\text{O}$  dips to approximately 45% of the initial ISM ratio exists at a  $z/r$  of 0.16–0.2 at  $r = 0.1\text{--}1$  au, as seen in Figure 1. The upper boundary of this layer corresponds to where  $\text{CO}$  becomes optically thick enough to self-shield, producing an environment where  $\text{C}^{18}\text{O}$  continues to photodissociate while  $\text{C}^{16}\text{O}$  does not, releasing free  $^{18}\text{O}$ . Much of the free  $^{18}\text{O}$  finds its way into water molecules, enhancing the  $\text{H}_2^{18}\text{O}$  abundance, thus providing a lower ratio between  $\text{H}_2\text{O}$  and  $\text{H}_2^{18}\text{O}$  ( $\approx 300$ ). The most common  $^{18}\text{O}$  destruction mechanisms come in the form of interactions with  $\text{H}_2$  to form  $^{18}\text{OH}$  and an extra H atom.  $^{18}\text{OH}$  can then interact with an  $\text{H}_2$  atom to form  $\text{H}_2^{18}\text{O}$ . The main cycle of  $^{18}\text{O}$  once the chemistry has reached equilibrium is shown in Figure 2. The ratio returns to an ISM level at  $z/r \approx 0.16$  when  $\text{C}^{18}\text{O}$  starts to be shielded, cutting off the supply of free  $^{18}\text{O}$ . Near the same  $z/r$ , within 1 au,  $\text{H}_2\text{O}$  UV-shielding aids in shielding  $\text{C}^{18}\text{O}$  to a point where its photodissociation rate is extremely low, many orders of magnitude lower than an environment where  $\text{H}_2\text{O}$  UV-shielding would be ignored.

Beyond  $\sim 1$  au, the water abundance drops, yet a non-ISM ratio still exists.  $\text{CO}$  self-shielding continues to dominate, continuing to produce a  $^{18}\text{O}$ -enhanced environment, thus a continued low ratio of  $\text{H}_2\text{O}$  to  $\text{H}_2^{18}\text{O}$ ; however, there exists very little water vapor in the gas phase beyond  $r = 1$  au. The  $\text{H}_2^{18}\text{O}$ -enhanced region exists between a top-down vertical  $\text{CO}$  column of  $10^{17}$  and  $10^{19} \text{ cm}^{-2}$ , an  $\text{H}_2$  column of  $10^{19}$  and  $10^{22} \text{ cm}^{-2}$ , and below an H column of  $10^{21} \text{ cm}^{-2}$ . This  $\text{H}_2^{18}\text{O}$ -enhanced region coexists with large temperature gradients. Within 1 au, the thermal range from the bottom of this

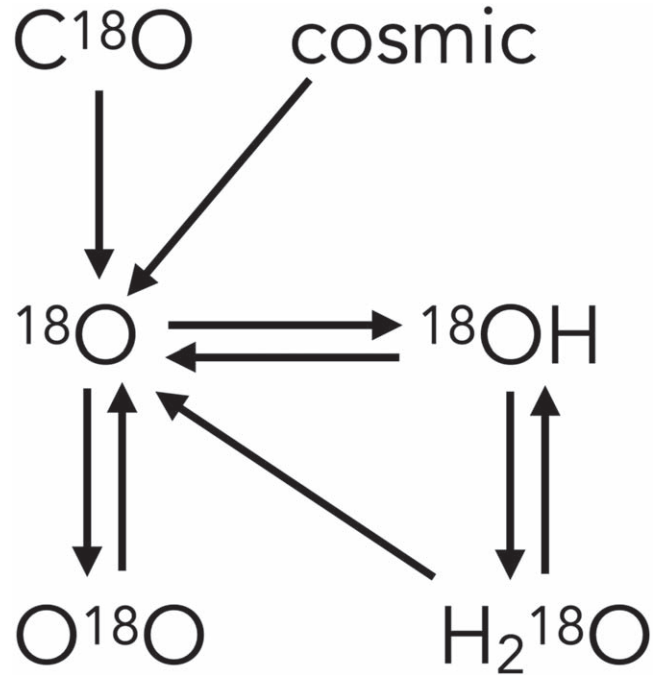


**Figure 2.** The evolution of  $^{18}\text{O}$  in equilibrium chemistry in the  $\text{H}_2^{18}\text{O}$ -enhanced region. Most of the oxygen comes from the dark cloud material originating from molecules like  $\text{H}_2\text{O}$ ,  $\text{CO}_2$ , organics, and silicates. In this region photodissociation of  $\text{C}^{18}\text{O}$  provides an elevated abundance of  $^{18}\text{O}$  that reacts with H and  $\text{H}_2$  to quickly form  $^{18}\text{OH}$  and  $\text{H}_2^{18}\text{O}$ . Because  $\text{C}^{16}\text{O}$  is shielded, very little extra  $^{16}\text{O}$  is included in this oxygen cycle, thus the relative increase in  $\text{H}_2^{18}\text{O}$  production.

layer to the top is 500–2000 K. Beyond 1 au the gradient is larger, ranging from 100 to 4000 K.

We find that most  $\text{Ly}\alpha$  photons do not reach the  $\text{H}_2$ -dominated zone of the disk, including where the  $\text{H}_2^{18}\text{O}$ -rich region exits. The  $\text{Ly}\alpha$  emission feature is 25 times less bright in

**Table 1**  
Transitions of  $\text{H}_2^{18}\text{O}$  Observable with JWST

Transition	Wavelength ( $\mu\text{m}$ )	$E_{\text{up}}$ (K)	$A$ ( $\text{s}^{-1}$ )	Weighted $^{16}\text{O}/^{18}\text{O}$ Average
$10_{(3,8)}-9_{(0,9)}$	19.08	2072.3	0.83	520
$13_{(5,8)}-12_{(4,9)}$	19.78	3772.5	8.9	500
$10_{(4,7)}-9_{(1,8)}$	20.01	2265.3	1.9	510
$11_{(4,7)}-10_{(3,8)}$	22.03	2725.3	4.4	490
$9_{(7,2)}-9_{(4,5)}$	22.77	2581.7	0.031	540
$9_{(9,0)}-8_{(8,1)}$	23.17	3165.9	41.	420
$9_{(6,3)}-8_{(5,4)}$	26.83	2329.5	15.	410
$8_{(7,2)}-7_{(6,1)}$	26.99	2265.6	21.	400

**Note.** We quote each weighted average of the  $^{16}\text{O}$ -to- $^{18}\text{O}$  ratio with two significant figures following the level of certainty around the ISM value (assumed to be 550).

the radiation field of the disk at the location of the  $\text{H}_2^{18}\text{O}$ -rich region than it would be if the transfer of  $\text{Ly}\alpha$  photons was disregarded. Despite the decrease in overall UV flux, the  $\text{H}_2^{18}\text{O}$ -rich region exits over the same spatial extent of the disk compared to a model that does not account for  $\text{Ly}\alpha$  scattering off of hydrogen atoms. The limit at which scattered  $\text{Ly}\alpha$  photons have a decreasing contribution to the radiation field corresponds to a  $z/r \approx 0.25$ , or where the H-to- $\text{H}_2$  ratio is  $\approx 10^{-5}$ . While in this disk model  $\text{Ly}\alpha$  did not reach into the molecular disk, Bethell & Bergin (2011) found that the molecular disk can be enhanced with  $\text{Ly}\alpha$  relative to FUV photons using the detailed disk physical models by D’Alessio et al. (2006). In this study, we use the thermochemical calculation within DALI and a chemical network to determine the H-fraction throughout the disk, while Bethell & Bergin (2011) used an analytical expression taking into account photodissociation and self-shielding processes while leaving out chemical destruction or creation pathways for  $\text{H}_2$  and H. This results in a H-to- $\text{H}_2$  transition within the work that exists higher in the disk as compared to Bethell & Bergin (2011). Additionally, in Bethell & Bergin (2011) the H-fraction drops to near zero while  $\text{H}_2$  is dominate, while in DALI there exists a population of free H atoms in the  $\text{H}_2$ -dominated region of the disk due to destructive chemical reactions. Thus, in the DALI disk, there are scattering events deep in the disk where in Bethell & Bergin (2011) there were none. The additional scattering events greatly increase the chance for  $\text{Ly}\alpha$  photons to be absorbed by dust.

### 3.2. $\text{H}_2^{18}\text{O}$ Emission Spectrum

The bulk of the water content exists within a radius of 1 au. We use DALI to calculate the flux contribution per cell for each emitted line. In order to determine which water lines will be of high interest, we run a quick non-LTE ray-tracing program (Bosman et al. 2017, Appendix B) that estimates the flux of water lines over the full extent of the MIRI wavelength range. We find that IR bright  $\text{H}_2\text{O}$  lines emit high up in the disk, proving to be optically thick across all IR wavelengths (see A. D. Bosman et al. 2022, in preparation for detail). Isolated and bright  $\text{H}_2^{18}\text{O}$  emission lines are rare, but a handful of lines will be accessible and distinguishable from  $\text{H}_2\text{O}$  with the MIRI instrument. We find eight distinct lines listed in Table 1 and highlighted in Figure 3. These lines exist between 19 and  $27 \mu\text{m}$ ; notably a region in MIRI with a lower sensitivity compared to shorter wavelength ranges.

Each  $\text{H}_2^{18}\text{O}$  line emits from distinct heights within the disk, and may partially emit from the  $\text{H}_2^{18}\text{O}$ -enhanced region; thus, when converting from  $\text{H}_2^{18}\text{O}$  emission to an  $\text{H}_2\text{O}$  abundance, a ratio below that of the ISM should be used. One of the brightest and most isolated lines is the  $\text{H}_2^{18}\text{O}$   $8_{(7,2)}-7_{(6,1)}$  ( $27 \mu\text{m}$ ) transition. We find that this transition starts to become optically thick and emits primarily in the enriched  $^{18}\text{O}$  region. We find this to be true for seven out of the eight identified lines. The  $\text{H}_2^{18}\text{O}$   $9_{(7,2)}-9_{(4,5)}$  transition ( $22.77 \mu\text{m}$ ) appears to primarily emit below the  $\text{H}_2^{18}\text{O}$ -enriched region; thus, if using this line to determine an  $\text{H}_2\text{O}$  abundance, the conversion factor will be closer to an ISM value of 550.

## 4. Discussion and Analysis

### 4.1. Measuring $\text{H}_2\text{O}$ Abundance Using $\text{H}_2^{18}\text{O}$ Observations

A weighted ratio between  $\text{H}_2\text{O}$  and  $\text{H}_2^{18}\text{O}$  must be used in order to extrapolate to an  $\text{H}_2\text{O}$  abundance and distribution using  $\text{H}_2^{18}\text{O}$  observations. We have identified eight transitions of  $\text{H}_2^{18}\text{O}$  that are observable with JWST, and calculate the weighted ratio of  $\text{H}_2\text{O}$  to  $\text{H}_2^{18}\text{O}$  that should be assumed based on our AS 209 model, and the vertical layers where we predict the emission arises. We compute weighted averages of  $\text{H}_2\text{O}/\text{H}_2^{18}\text{O}$  using the relative spatial contribution from where each line is emitting from, as calculated by DALI.

Our first example comes from the  $\text{H}_2^{18}\text{O}$   $8_{(7,2)}-7_{(6,1)}$  transition at  $27 \mu\text{m}$ . As seen in Figure 4, much of the emission from this line originates from the  $\text{H}_2^{18}\text{O}$  enhanced region. We use the following equation to calculate a weighted  $\text{H}_2\text{O}/\text{H}_2^{18}\text{O}$  value:

$$W = \frac{\sum_{i=1}^n w_i \chi_i}{\sum_{i=1}^n w_i}, \quad (2)$$

where  $n$  is the number of cells in our model,  $w_i$  is the relative emission contribution in a cell, and  $\chi_i$  is the  $\text{H}_2\text{O}/\text{H}_2^{18}\text{O}$  value in a cell. Using this formalism, we find the average  $\text{H}_2\text{O}/\text{H}_2^{18}\text{O}$  coming from this transition is  $\sim 400$ . The  $\text{H}_2^{18}\text{O}$  at  $22.77 \mu\text{m}$  appears to emit from a drastically different region in the disk; thus, its average  $\text{H}_2\text{O}/\text{H}_2^{18}\text{O}$  is 540, nearly identical within the margin of error to the typically used ISM estimate. We list the calculated weighted averaged determined for the eight identified bright and isolated  $\text{H}_2^{18}\text{O}$  transitions in Table 1. There is a general trend that transitions from smaller wavelengths trend toward a weighted average of 550. This trend arises from the Einstein A-coefficient associated with each transition. Transitions with lower  $A$  values are more likely to emit from deeper within the disk at higher gas densities, thus farther away from the  $\text{H}_2^{18}\text{O}$ -enhanced region. To reduce the uncertainty in the  $\text{H}_2\text{O}/\text{H}_2^{18}\text{O}$  ratio, transitions associated with low Einstein A-coefficients could be preferentially used. These differences are small and up to a factor of 2. However, chemical studies will be looking for enhanced abundances of water vapor in this region, perhaps supplied by pebble drift (Banzatti et al. 2020). To isolate these chemical changes we need to correct for effects that can be understood; water UV-shielding is one of these effects.

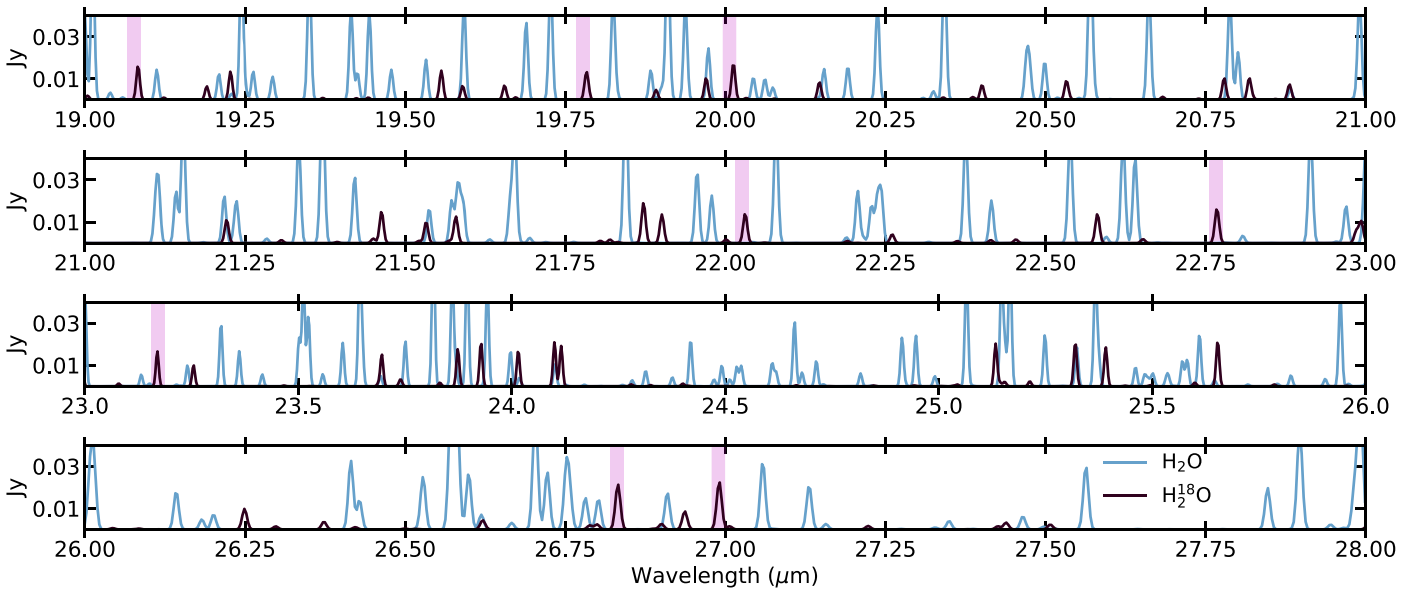


**Figure 3.** The  $\text{H}_2\text{O}$  and  $\text{H}_2^{18}\text{O}$  spectra as predicted from an AS 209 model including water UV-shielding and  $\text{Ly}\alpha$  contributions with  $0.1 \text{ km s}^{-1}$  velocity bins. Blue lines correspond to  $\text{H}_2\text{O}$  and dark purple with  $\text{H}_2^{18}\text{O}$ .  $\text{H}_2^{18}\text{O}$  lines that are relatively bright and isolated from  $\text{H}_2\text{O}$  lines are highlighted.

#### 4.2. Corresponding CO Infrared Observations

In the  $\text{H}_2^{18}\text{O}$ -enhanced region,  $\text{C}^{18}\text{O}$  abundance drops and the  $^{12}\text{CO}$ -to- $\text{C}^{18}\text{O}$  ratio increases by upward of four orders of magnitude. Measuring the  $^{12}\text{CO}$ -to- $\text{C}^{18}\text{O}$  ratio using lines of CO that emit from this region could help confirm the presence of this  $^{18}\text{O}$ -rich region and even calibrate uncertainties in the true ratio between  $\text{H}_2\text{O}$  and  $\text{H}_2^{18}\text{O}$ . The R and P branches for multiple vibrational transitions of CO and its isotopologues peak at  $\sim 5 \mu\text{m}$  and are observable from the ground using high spectral resolution instruments such as Keck NIRSPEC and the Very Large Telescope’s CRIRES. The  $\text{C}^{18}\text{O}$  column densities in the  $\text{H}_2^{18}\text{O}$ -rich region range from  $10^{12}$  to  $10^{15} \text{ cm}^{-2}$  and are predicted to produce optically thin  $\text{C}^{18}\text{O}$  emission in the infrared. As summarized and expanded upon in Banzatti et al. (2022), over 100 T Tauri and Herbig disks have been observed with high spectral resolution in the wavelength range of CO’s vibrational lines which emit from  $\sim 1000 \text{ K}$ , corresponding to the temperature of the  $\text{H}_2^{18}\text{O}$ -enhanced region. In these studies only CO and  $^{13}\text{CO}$  observations were reported, making it currently impossible to use these observations to corroborate our predicted  $^{18}\text{O}$ -rich region within 1 au. The only work that set out to measure  $^{12}\text{CO}/\text{C}^{18}\text{O}$  and  $^{12}\text{CO}/\text{C}^{17}\text{O}$  is found in Smith et al. (2015). This study observed nine young stellar objects (YSOs), three of which were optically thick disks. These three disks show tentative increase in the  $^{12}\text{CO}/\text{C}^{18}\text{O}$  well above the ISM-measured value; however, it was noted that significant systematic uncertainties were associated with these measurements. A future study dedicated to deep observations of multiple disk systems could aid in upcoming MIRI observations of these regions, and put constraints on the  $^{18}\text{O}$  enhancement within the radial extent of planet formation.

#### 4.3. Impact of a Different $^{16}\text{O}/^{18}\text{O}$ Ratio

Mass-independent fractionation of oxygen isotopes, with enrichment of the heavy isotopes, has been isolated within meteoritic material (Clayton et al. 1973; Thieme & Heidenreich 1983). The origin of these isotopic anomalies requires a specific mechanism that creates an  $^{18}\text{O}$ -rich (and

$^{17}\text{O}$ -rich) environment as compared to the natal stellar nebula and envelope (Clayton 1993). This fractionation must originate in the solar nebular disk or within the natal molecular cloud (Yurimoto & Kuramoto 2004; Lyons & Young 2005; Lee et al. 2008). CO self-shielding presents a mechanism to enrich gas in heavy isotopes, particularly on surfaces exposed to ultraviolet, as it selectively photodissociates  $\text{C}^{18}\text{O}$  and  $\text{C}^{17}\text{O}$  relative to CO producing gas enriched in  $^{18}\text{O}$  and  $^{17}\text{O}$  (Lyons & Young 2005; Miotello et al. 2014). In this work, we find that the addition of  $\text{H}_2\text{O}$  UV-shielding not only continues the  $^{18}\text{O}$  enrichment within the inner disk, but enhances it compared to results solely based on CO self-shielding. We find a depletion of  $\text{C}^{18}\text{O}$  approaching a factor of  $10^3$  high up in the disk between 0.1–30 au at a  $\sim z/r = 0.2$ –0.3. This is a reservoir rich with  $^{18}\text{O}$ , enhancing the  $^{18}\text{O}$  isotopologues for many different volatile species, including water vapor and ice.

Vertical mixing may act as a mechanism to deliver the  $^{18}\text{O}$ -enhanced molecules to the planet-forming midplane. The “cold finger” effect (Stevenson & Lunine 1988; Meijerink et al. 2009) has been proposed a mechanism that will transport water and other organics efficiently from the atmosphere of the disk to the midplane. Due to vertical mixing, water from the gaseous atmosphere can transport down to the midplane where it locked onto grains as ice. The cold finger effect has been used to reconcile models in which high water abundances are predicted, yet corresponding submillimeter observations exhibit nondetections (Salyk et al. 2011; Du et al. 2015; Carr et al. 2018; Bosman & Bergin 2021; Bosman et al. 2022). Thus, while the  $\text{H}_2^{18}\text{O}$ -rich regions reside high up in the disk atmosphere, vertical mixing can bring a portion of this reservoir down to the midplane and enrich meteoritic precursors.

Lyons & Young (2005) explored a solution in the outer tens of astronomical units that suggested that meteoritic  $^{18}\text{O}$  enrichment could be the result of CO self-shielding. In this model, oxygen atoms (enriched with heavy isotopes) produced via isotopic-selective CO self-shielding, are mixed downward forming water ice via grain surface chemistry. These ices will need to be transported to the inner few astronomical units,

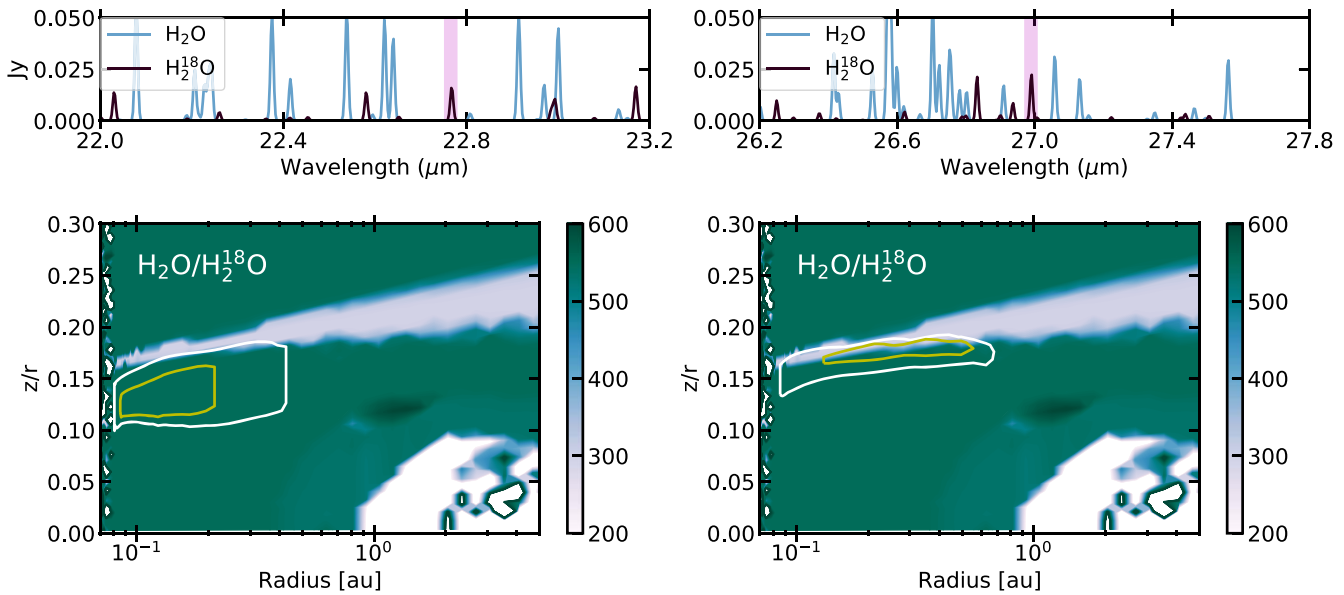


**Figure 4.** Top: the overlapping spectra from  $\text{H}_2\text{O}$  and  $\text{H}_2^{18}\text{O}$  focusing on a narrow wavelength regions within the MIRI instrument on JWST, focused on the  $\text{H}_2^{18}\text{O}$  27  $\mu\text{m}$  line (left) and 22.77  $\mu\text{m}$  (right) lines. Bottom: the 50% (yellow contour) and 90% (white contour) contribution regions for each line plotted over the  $\text{H}_2\text{O}$ -to- $\text{H}_2^{18}\text{O}$  ratio.

perhaps by drift (Ciesla & Cuzzi 2006). However, current meteoritic evidence suggests the inner solar system is chemically separated from the outer ( $\gtrsim 5$  au) parts of the disk between 1 Myr and 3–4 Myr, potentially due to early formation of Jupiter’s core (Kruijer et al. 2017). Our model shows that this vertical layer of enhanced  $^{18}\text{O}$  is placed directly into water in surface layers above the inner disk spatially closer to the region where meteoritic progenitors originate.

## 5. Conclusion

In this Letter, we implement  $\text{H}_2\text{O}$  UV-shielding and chemical heating in addition to CO self-shielding within a gas-rich disk environment. Focusing on the innermost region of the disk, a water vapor-rich reservoir exits within 1 au, and a  $\text{H}_2^{18}\text{O}$ -enhanced region exists where many water IR lines approach a  $\tau = 1$ . In this region, the  $\text{H}_2\text{O}$ -to- $\text{H}_2^{18}\text{O}$  ratio approaches 300, a significantly lower value than the assumed ISM ratio of 550. We then seek to use this context to provide insight into future JWST observations of  $\text{H}_2^{18}\text{O}$  as it will act as a tracer for the abundance and distribution of gaseous  $\text{H}_2\text{O}$  in the main planet formation zone.

1. In our disk model, the  $\text{H}_2\text{O}$ -to- $\text{H}_2^{18}\text{O}$  ratio approaches 300 between a  $z/r \approx 0.16$ – $0.2$  and inside 1 au due to CO self-shielding.
2. We identify eight bright and isolated  $\text{H}_2^{18}\text{O}$  lines that can be used to access the abundance and distribution of  $\text{H}_2\text{O}$ . Transitions associated with higher Einstein A-coefficients such as  $\text{H}_2^{18}\text{O } 8_{(7,2)} - 7_{(6,1)}$  at 27  $\mu\text{m}$  emit, primarily in the  $\text{H}_2^{18}\text{O}$ -rich region; thus, the ratio between  $\text{H}_2\text{O}$  and  $\text{H}_2^{18}\text{O}$  is less than the local ISM value of 550. Seven out of the eight identified transitions emit predominately from the  $\text{H}_2^{18}\text{O}$ -enhanced region; thus, most observable  $\text{H}_2^{18}\text{O}$  transitions with JWST will have an additional factor of uncertainty when converting  $\text{H}_2^{18}\text{O}$  abundance to  $\text{H}_2\text{O}$ .
3. In this model Ly $\alpha$  radiation does not penetrate down to the molecular-rich region of the disk in the case of our relatively thin and  $0.0045 M_{\odot}$  disk.

4. Vertical diffusive mixing, or the “cold finger” effect, could transport a significant amount of  $^{18}\text{O}$ -rich molecules to the planet-forming midplane to be incorporated into preplanetary materials that reside in the terrestrial planet-forming zone.

J.K.C. acknowledges support from the National Science Foundation Graduate Research Fellowship under grant No. DGE 1256260 and the National Aeronautics and Space Administration FINESST grant, under grant No. 80NSSC19K1534.

A.D.B. and E.A.B. acknowledge support from NSF grant No. 1907653 and NASA grant XRP 80NSSC20K0259.

*Software:* DALI (Bruderer et al. 2012; Bruderer 2013), scipy (Virtanen et al. 2020), Matplotlib (Hunter 2007), Astropy (Astropy Collaboration et al. 2013, 2018), NumPy (Harris et al. 2020), RADMC-3D (Dullemond et al. 2012), radmc3dPy ([https://bitbucket.org/at\\_juhasz/radmc3dpy/](https://bitbucket.org/at_juhasz/radmc3dpy/)), parallel (Tange 2018).

## ORCID iDs

Jenny K. Calahan <https://orcid.org/0000-0002-0150-0125>  
 Edwin A. Bergin <https://orcid.org/0000-0003-4179-6394>  
 Arthur D. Bosman <https://orcid.org/0000-0003-4001-3589>

## References

- Altwegg, K., Balsiger, H., Combi, M., et al. 2020, *MNRAS*, **498**, 5855  
 Astropy Collaboration, Price-Whelan, A. M., Sipőcz, B. M., et al. 2018, *AJ*, **156**, 123  
 Astropy Collaboration, Robitaille, T. P., Tollerud, E. J., et al. 2013, *A&A*, **558**, A33  
 Banzatti, A., Abernathy, K. M., Brittain, S., et al. 2022, *AJ*, **163**, 174  
 Banzatti, A., Pascucci, I., Bosman, A. D., et al. 2020, *ApJ*, **903**, 124  
 Bethell, T., & Bergin, E. 2009, *Sci*, **326**, 1675  
 Bethell, T. J., & Bergin, E. A. 2011, *ApJ*, **739**, 78  
 Bosman, A. B., Bergin, E. A., Calahan, J. K., & Duval, S. 2022, *ApJL*, **930**, L26  
 Bosman, A. D., & Bergin, E. A. 2021, *ApJL*, **918**, L10  
 Bosman, A. D., Bruderer, S., & van Dishoeck, E. F. 2017, *A&A*, **601**, A36  
 Brittain, S. D., Rettig, T. W., Simon, T., & Kulesa, C. 2005, *ApJ*, **626**, 283  
 Bruderer, S. 2013, *A&A*, **559**, A46

- Bruderer, S., van Dishoeck, E. F., Doty, S. D., & Herczeg, G. J. 2012, *A&A*, **541**, A91
- Carr, J. S., & Najita, J. R. 2008, *Sci*, **319**, 1504
- Carr, J. S., Najita, J. R., & Salyk, C. 2018, *RNAAS*, **2**, 169
- Ciesla, F. J., & Cuzzi, J. N. 2006, *Icar*, **181**, 178
- Clayton, R. N. 1993, *AREPS*, **21**, 115
- Clayton, R. N., Grossman, L., & Mayeda, T. K. 1973, *Sci*, **182**, 485
- D'Alessio, P., Calvet, N., Hartmann, L., Franco-Hernández, R., & Servín, H. 2006, *ApJ*, **638**, 314
- Du, F., Bergin, E. A., & Hogerheijde, M. R. 2015, *ApJL*, **807**, L32
- Dullemond, C. P., Juhasz, A., Pohl, A., et al. 2012, *ascl.soft: 1202.015*
- Faure, A., & Josselin, E. 2008, *A&A*, **492**, 257
- Gordon, I. E., Rothman, L. S., Hargreaves, R. J., et al. 2022, *JQSRT*, **277**, 107949
- Gundlach, B., & Blum, J. 2015, *ApJ*, **798**, 34
- Harris, C. R., Millman, K. J., van der Walt, S. J., et al. 2020, *Natur*, **585**, 357
- Heays, A. N., Bosman, A. D., & van Dishoeck, E. F. 2017, *A&A*, **602**, A105
- Herczeg, G. J., Linsky, J. L., Valenti, J. A., Johns-Krull, C. M., & Wood, B. E. 2002, *ApJ*, **572**, 310
- Houck, J. R., Roellig, T. L., Van Cleve, J., et al. 2004, *Proc. SPIE*, **5487**, 62
- Hunter, J. D. 2007, *CSE*, **9**, 90
- Johnson, J. A., Aller, K. M., Howard, A. W., & Crepp, J. R. 2010, *PASP*, **122**, 905
- Kruijjer, T. S., Burkhardt, C., Budde, G., & Kleine, T. 2017, *PNAS*, **114**, 6712
- Lee, J.-E., Bergin, E. A., & Lyons, J. R. 2008, *M&PS*, **43**, 1351
- Lyons, J. R., & Young, E. D. 2005, *Natur*, **435**, 317
- Meijerink, R., Pontoppidan, K. M., Blake, G. A., Poelman, D. R., & Dullemond, C. P. 2009, *ApJ*, **704**, 1471
- Miotello, A., Bruderer, S., & van Dishoeck, E. F. 2014, *A&A*, **572**, A96
- Mulders, G. D., Pascucci, I., Apai, D., & Ciesla, F. J. 2018, *AJ*, **156**, 24
- Nittler, L. R., & Gaidos, E. 2012, *M&PS*, **47**, 2031
- Pontoppidan, K. M., Salyk, C., Bergin, E. A., et al. 2014, in *Protostars and Planets VI*, ed. H. Beuther et al. (Tucson, AZ: Univ. Arizona Press), 363
- Pontoppidan, K. M., Salyk, C., Blake, G. A., et al. 2010, *ApJ*, **720**, 887
- Rieke, G. H., Wright, G. S., Böker, T., et al. 2015, *PASP*, **127**, 584
- Salyk, C., Pontoppidan, K. M., Blake, G. A., Najita, J. R., & Carr, J. S. 2011, *ApJ*, **731**, 130
- Schindhelm, R., France, K., Herczeg, G. J., et al. 2012, *ApJL*, **756**, L23
- Schöier, F. L., van der Tak, F. F. S., van Dishoeck, E. F., & Black, J. H. 2005, *A&A*, **432**, 369
- Smith, R. L., Pontoppidan, K. M., Young, E. D., & Morris, M. R. 2015, *ApJ*, **813**, 120
- Smith, R. L., Pontoppidan, K. M., Young, E. D., Morris, M. R., & van Dishoeck, E. F. 2009, *ApJ*, **701**, 163
- Stevenson, D. J., & Lunine, J. I. 1988, *Icar*, **75**, 146
- Tange, O. 2018, 2018, GNU Parallel, Zenodo doi:10.5281/zenodo.1146014
- Thiemens, M. H., & Heidenreich, J. E. 1983, *Sci*, **219**, 1073
- van Dishoeck, E. F., & Black, J. H. 1988, *ApJ*, **334**, 771
- van Dishoeck, E. F., Jonkheid, B., & van Hemert, M. C. 2006, *FaDi*, **133**, 231
- Virtanen, P., Gommers, R., Oliphant, T. E., et al. 2020, *Nat. Methods*, **17**, 261
- Wang, H., Bell, R. C., Iedema, M. J., Tsekouras, A. A., & Cowin, J. P. 2005, *ApJ*, **620**, 1027
- Wilson, T. L. 1999, *RPPH*, **62**, 143
- Wilson, T. L., & Rood, R. 1994, *ARA&A*, **32**, 191
- Yurimoto, H., & Kuramoto, K. 2004, *Sci*, **305**, 1763
- Zhang, K., Booth, A. S., Law, C. J., et al. 2021, *ApJS*, **257**, 5